Journal of Forestry Research (2026) 37:34
https://doi.org/10.1007/s11676-025-01979-9

ORIGINAL PAPER

Methods for identifying topkill in conifers using airborne lidar to monitor structural diversity and disturbance

Brent W. Oblinger[1] · **Benjamin C. Bright**[2] · **Andrew T. Hudak**[2] · **Kerri T. Vierling**[3]

Received: 5 November 2024 / Accepted: 13 March 2025 / Published online: 5 January 2026

Abstract Forest insects and pathogens, in addition to fire, contribute to structural diversity by creating snags (dead trees) and dead tops on live trees or "topkill" in conifers throughout western North America. Snags and top-killed trees are important sources of wildlife habitat but quantifying their presence can be challenging at broad scales. Multiple approaches for detecting snags have been developed, but limited methods exist for detecting topkill via remote sensing. There is a need to monitor overlapping disturbances across time and space in addition to the structural diversity in mature and old-growth forests. We used airborne light detection and ranging (lidar) and associated field observations to map individual dead trees and live trees with topkill across a forest dominated by *Pinus ponderosa* in central Oregon. The lidar point cloud was segmented into individual tree objects (polygons representing tree crown extents as viewed from nadir), for which lidar metrics were computed. Lidar-detected tree objects were paired with 647 field-observed trees with corresponding tree health measurements, and a random forest classifier was developed that separated trees into: (1) live without topkill; (2) live with topkill; and (3) dead classes with 87% accuracy using lidar metrics. Tree mortality was mainly due to fire injury and native bark beetles, such as western pine beetle (*Dendroctonus brevicomis*), while topkill was primarily due to comandra blister rust (caused by the native fungal pathogen *Cronartium comandrae*). The classifier was applied to map individual tree health status for 46,444 tree objects from which tree health class density maps were created across the 229-ha study area. Approximately 43% were classified as live without topkill, 22% of trees were classified as live with topkill, and 35% of trees were classified as dead. This approach can be used to improve detection of topkill in conifers, along with tree mortality, caused by disturbances associated with forest insects and pathogens.

Keywords Remote sensing · Snags · Topkill · *Pinus ponderosa* · *Cronartium comandrae*

Project Funding: Funding for the airborne lidar acquisition was provided by the USDA Forest Service -Western Wildland Environmental Threat Assessment Center (WWETAC) and we appreciate Nancy E. Grulke. This research was supported (in part) by the U.S. Department of Agriculture, Forest Service. We greatly appreciate the assistance of Brian M. Wing (deceased), Kelly Smith, Paul Deignan and other USDA Forest Service staff that helped with field data collection. We are grateful for our colleague, Brian M. Wing who was also interested in improved detection of topkill along with our group in the past.

The online version is available at https://link.springer.com/.

Corresponding editor: Lei Yu.

✉ Brent W. Oblinger
brent.oblinger@usda.gov

[1] Forest Health Protection, USDA Forest Service, 63095 Deschutes Market Rd, Bend, OR 97701, USA

[2] Rocky Mountain Research Station, USDA Forest Service, 1221 South Main St, Moscow, ID 83844, USA

[3] Department of Fish and Wildlife Sciences, University of Idaho, 875 Perimeter Drive, Moscow, ID 83844, USA

Introduction

Evaluating structural diversity in forests is vital when considering the need for restoration treatments in dry, interior forests where large, old trees are often under-represented compared to historic conditions in many parts western North America (Hagmann et al. 2013; Kolb et al. 2007; Spies et al. 2006). Monitoring tree mortality levels and individual tree

health at the stand scale is also necessary to assess the risk of losing highly valued, old-growth characteristics due to disturbances associated with fire, a changing climate, competitive stress, insects and diseases (Dolph et al. 1995; Fiedler et al. 2007; Mercer et al. 2022; Perrakis et al. 2011). Understanding stand structure shaped by disturbances, or the absence of disturbance, in stands with large, old ponderosa pine is important to help inform management decisions (Harrod et al. 1999; Youngblood et al. 2004).

Standing dead trees (snags) contribute to structural diversity thereby enhancing wildlife habitat diversity and a variety of ecosystem services (Harmon et al. 2004; Kilgo and Vukovich 2014; Sandström et al. 2019). Size, abundance and stage of decomposition of snags are common structural indicators of available habitat, and indicators of biodiversity, when evaluating conditions for a range of habitat features (Marcot et al. 2010; Thomas et al. 1979; Bell et al. 2021). Quantifying the density of live and dead trees also helps to inform estimates of suitable habitat, biomass, carbon storage capacity of forests, timber volume, and potential fire behavior (Janisch and Harmon 2002; Lutz et al. 2021; Reed et al. 2023; Sánchez Meador et al. 2015).

The diversity of dead wood structures also influences forest biodiversity (Harmon et al. 2004; Sandström et al. 2019). Dead tops on live trees (topkill) contribute to structural diversity and enhance habitat availability through additional dead wood recruitment on living trees. For example, a variety of wildlife, including cavity-excavating birds, utilize live trees with topkill (Raphael and White 1984). The cavities excavated by different woodpecker species in topkill have wide-ranging influences on the wildlife community; for instance, Bunnell (2013) notes that over 60 species of vertebrates use these cavities for either roosting or nesting in the Pacific Northwest, and Hardin et al. (2021) suggest that woodpecker activities might have additional effects on trophic relationships within forested systems.

In addition to cavity excavations, the gaps that are created at the top of the canopy via tree mortality and topkill can influence foraging activities for multiple species. Topkill can provide perch sites and associated openings in the canopy are helpful for visual detection of prey, and bird species such as Lewis's woodpeckers (*Melanerpes lewis*) and olive-sided flycatchers (*Contopus cooperi*) have been noted to use topkill as perch sites from which to flycatch in the adjacent canopy gap (Altman and Sallabanks 2020; Vierling et al. 2020). Bats are also aerial insectivores and bat foraging behaviors are based on combinations of echolocation characteristics, wing morphologies, and foraging strategies, and fine scale canopy structural characteristics. While it is currently unknown whether bats forage around topkill sites, canopy gaps are known to influence the foraging behavior of some bat species (e.g. Jung et al. 2012; Froidevaux et al. 2016).

Detecting live trees with topkill and snags is important to monitor changes in live tree health, mortality levels, and other forest conditions before and after disturbances. Forest insects and diseases cause topkill on live trees that remain living for some time and identifying live conifers with topkill is important when evaluating the range of habitat features, or when estimating timber volume and merchantability (Cedervind and Långström 2003; Filip 1977; Geils and Jacobi 1993; Mitchell and Buffam 2001). Quantifying topkill is of particular interest when assessing tree vigor in stands with late, old-growth structure as large trees are often highly valued resources that take centuries to replace (Kolb et al. 2007; Spies et al. 2006).

In ponderosa pine, multiple insects and diseases can cause topkill in mature trees. Throughout many parts of western North America, the Ips pine engraver (*Ips pini*) and other *Ips* spp. can kill tops of pines after boring in the phloem (Furniss and Carolin 1977). The disease comandra blister rust, caused by a native fungal pathogen (*Cronartium comandrae*), affects two- and three-needle (hard) pines in North America and can cause topkill in lodgepole and ponderosa pines in the western U.S. (Bergdahl and French 1976; Filip 1977; Geils and Jacobi 1993; Miller and Blomstrom 1968; Powell 1970).

Comandra blister rust causes stem-girdling branch and bole cankers following infection by basidiospores in needles or young shoots of hard pines (Johnson 1979, 1986; Geils and Jacobi 1990). In addition to requiring a hard pine host, *Cronartium comandrae* is a heterocyclic rust fungus that requires an alternate host to complete its life cycle, such as comandra or bastard toadflax (*Comandra umbellata*), and northern comandra (*Geocaulon lividum*) (Johnson 1986). Individual branches on pines are killed as the obligate parasite causes expanding cankers, or entire portions of the crown can be killed after girdling and insect attacks around cankers (Jacobi 1993; Childs 1968). Bole cankers can also be lethal depending on where a bole canker occurs, and depending on the size of tree infected with seedlings and saplings more likely to be killed by bole cankers (Johnson 1986; Geils and Jacobi 1993). Cankers originating farther from the bole are also less likely to reach the bole and become lethal (Childs 1968; Geils and Jacobi 1990). In the U.S., topkill can be locally severe in lodgepole and ponderosa pines in parts of Rocky Mountains and the Cascades Range (Childs 1968; Johnson 1986).

Various methods for remote detection of snags have been developed to support monitoring efforts estimating the occurrence and density of snags (e.g. Meddens et al. 2011; Coleman et al. 2018; Wing et al. 2015; Krzystek et al. 2020; Oblinger et al. 2022; Monahan et al. 2022; Stitt et al. 2022a, b; Shrestha et al. 2024). Snag classification methods most often employ supervised classification, in which an analyst identifies tree health classes

(live or dead) in imagery or point cloud data (often with associated ground observations) and develops a statistical model predicting tree health status from metrics derived from remote sensing data. Fitted statistical models are then applied across remote sensing data extents to map tree health. Previous studies that classified high-resolution multispectral imagery have reported accuracies of ≥ 90% for distinguishing live and dead tree pixels. Point cloud data methodologies in which individual tree crown objects are detected and characterized have reported similar classification accuracies of ≥ 90% and snag detection rates ranging from 43 to 100%. While the remote detection of snags has been well studied, to our knowledge, only one previous study has investigated the remote detection of topkill with point cloud data; Shrestha et al. (2024) demonstrated the use of multispectral drone imagery, from which they generated three-dimensional point cloud data, for the detection of insect-caused tree damage in individual conifers. They were able to successfully distinguish six levels of tree damage with an overall accuracy of 70% and measure topkill in individual trees.

The objective of this study was to evaluate a method for remote detection of live conifers with topkill, live trees without topkill, and snags utilizing airborne lidar and a random forest classifier on a forested landscape. To examine this approach, a known location was used containing a mix of conifers with healthy crowns, live conifers with topkill and snags (Filip 1977).

Materials and methods

Study area

The Metolius Research Natural Area (RNA) covers 548 ha (1354 acres) on the eastern slope of the Cascades in the Deschutes National Forest (NF) in central Oregon, USA (center coordinates of 44.4939° N, 121.6196° W; Fig. 1). Forest stands are primarily comprised of mature ponderosa pine (*Pinus ponderosa*). Although ponderosa pine is the dominant tree species, Douglas-fir (*Pseudotsuga menziesii*), grand fir (*Abies grandis*), incense cedar (*Calocedrus decurrens*), and western larch (*Larix occidentalis*) also occur across the RNA. Terrain is flat on the western half of the RNA, with elevations ranging from 850 to 980 m (2789–3281 ft) above sea level. The eastern half of the RNA is a western-facing slope that ranges from 980 to 1490 m (3281–4888 ft) above sea level. Average annual precipitation is 660 mm, with little precipitation from June through September. Mean maximum and minimum temperatures in July are 27 and 8 °C, respectively. Mean maximum and minimum temperatures in January

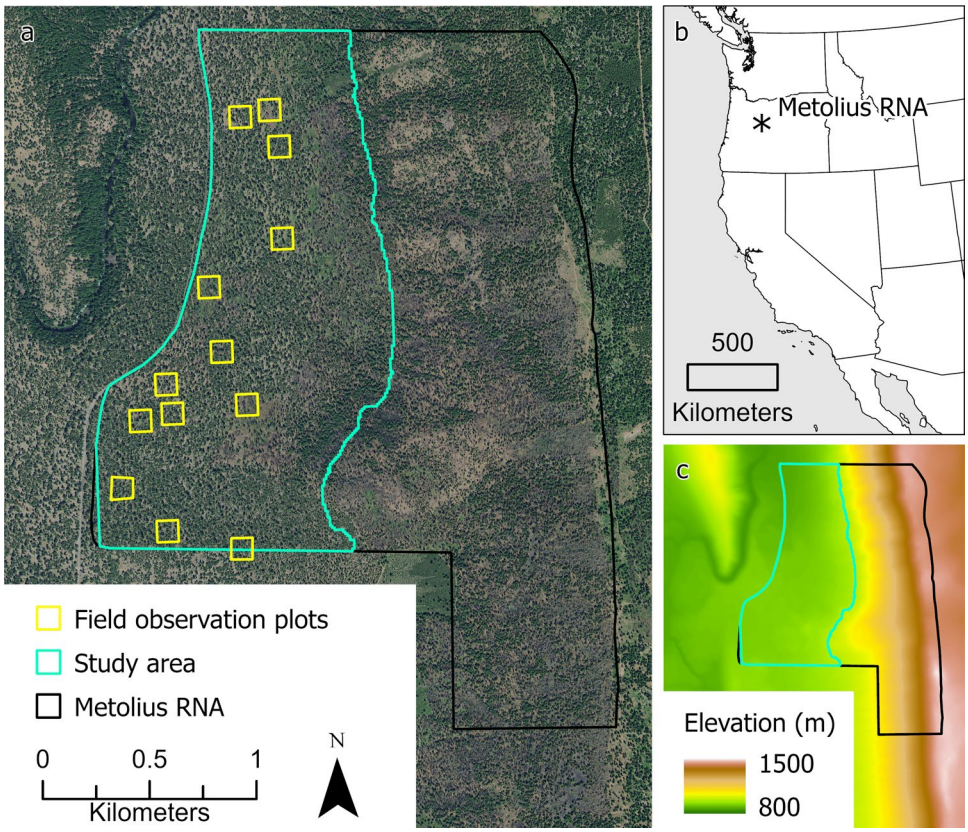

Fig. 1 Field observation plot locations within Metolius Research Natural Area (RNA) overlaid on true-color National Agriculture Imagery Program (NAIP) imagery from 2016 (panel a). Metolius RNA is located within the Deschutes National Forest (NF) in central Oregon, USA (panel b). The analysis was constrained to the western portion of the RNA highlighted where plots were installed and terrain was relatively flat with elevation ranging 850–980 m above sea level (panel c)

are 5 and –4 °C, respectively (1991–2020 climate normals from PRISM, https://prism.oregonstate.edu/normals/). We restricted our analysis to the flatter western portion of the RNA where field observation plots were located, elevation above sea level was < 980 m, and ponderosa pine is the dominant tree species.

Field observations

Field observations of 1120 trees, which were almost exclusively ponderosa pine, were gathered on 13 long-term monitoring plots located in the western half of the RNA in the summers of 2016 and 2017 (Fig. 1). Long-term monitoring plots were square with an area of 1 ha (100 m × 100 m). Tree status (live or dead), tree height, the presence and height of topkill on live trees (Fig. 2), and tree location relative to GNSS-measured plot corner locations were recorded for each tree with a diameter at breast height (DBH; 1.37 m) > 12.7 cm. The cause of tree mortality or topkill was recorded when discernable. Professional-grade GNSS receivers with sub-meter estimated horizontal accuracy after differential correction were used to record plot locations from which tree locations were determined. Field observations were converted to point shapefile format for intersection with lidar-derived tree objects.

Fig. 2 Ponderosa pine (*Pinus ponderosa*) with and without topkill in the Metolius Research Natural Area, central Oregon

Airborne lidar data acquisition and processing

Airborne lidar data were acquired across Metolius RNA in the fall of 2016 (Table 1). The vendor delivered point cloud data as LAS files in which returns were classified as ground or nonground. Ground-classified returns were interpolated to create a digital terrain model (DTM) with FUSION software (McGaughey 2022). The DTM heights were then subtracted from heights of the aboveground returns to create height-normalized LAS files in which elevation values represented heights above ground. Height-normalized LAS files were compressed to LAZ files and merged into one LAZ file with LAStools software (Isenburg 2020).

Discrete-return lidar systems often record multiple returns per pulse, so that intensity, or the amount of energy returned to the lidar sensor, gets distributed among multiple returns. To account for this possible confounding effect when using lidar intensity for analysis, we used only first returns, i.e., returns where the Return Number LAZ field = 1. We also considered using only single returns, in which the laser pulse is reflected by a single surface and not distributed among multiple returns, indicated by returns where the Number of Returns LAZ field = 1. However, we found no improvement in using only single returns versus first returns for our classification analysis. In addition to return number, intensity variation caused by automatic gain control (AGC) and range variation can introduce confounding effects when lidar intensity data is used for analysis (Korpela et al. 2010). To determine whether intensity artifacts were present in our data, we produced 10-m mean and maximum intensity rasters across the lidar acquisition and examined these grids for possible artifacts. The AGC artifacts that can manifest as artificial striping did not appear to be present in intensity

Table 1 Lidar acquisition parameters

Parameter	Value
Vendor	Atlantic Group, LLC
Aircraft	Cessna T210L (N732JE) or Partenavia S.P.A. P 68 C/TC (N775MW)
Lidar system	Leica ALS70-HP
Nominal flight height	1965 m aboveground level
Sensor scan angle	30°
Scan frequency	41 Hz
Pulse rate of scanner	278 kHz
Laser wavelength	1064 nm
Beam divergence	0.22 mrad
Nominal swath width	1098 m
Nominal swath overlap	50%
Nominal pulse density	4.6 pulses m^{-2}
Return density	17 returns m^{-2}

rasters, suggesting the vendor's proprietary process for removing the influence of AGC on intensity values, which we requested to be completed, was successful. We also found that no relationship between elevation above sea level and maximum and mean lidar intensity grids across the study area, suggesting that range normalization was not necessary.

A canopy height model (CHM) with a spatial resolution of 1 m was created from the height-normalized LAZ file with the 'rasterize_canopy' and 'p2r' functions of the 'lidR' R package (R Core Team 2022; Roussel et al. 2020; Roussel and Auty 2022). Individual tree tops were identified within the CHM using a local maximum filter (lmf) function implemented in the 'locate_trees' function of the 'lidR' package. To optimize lmf parameters for our study area, we based the circular moving window diameter for detecting CHM maxima on a linear model predicting crown diameter from tree height in our study area (Popescu and Wynne 2004). We determined optimal linear model coefficients by running several iterations of the 'locate_trees' function with differing lmf window sizes for the entire acquisition. For each iteration, we calculated crown diameters and tree heights for all detected tree objects ($n = 22{,}000$–$53{,}000$) and fit a linear model ($R^2 = 0.35$–0.42) predicting crown diameter from tree height. We chose a final lmf function (Fig. 3) that averaged linear model parameters for the various linear models without resulting in overly segmented tree crowns, as determined by visual inspection of tree crown objects:

$$ws = 1.5 + h \times 0.2 \quad (1)$$

where ws is the diameter of the moving window size (m) for detecting CHM maxima, based on the average crown diameter for a tree of height (h), or the height of the CHM (m). The 'locate_trees' function was run with Eq. 1 as the lmf function for final identification of individual tree tops across the CHM.

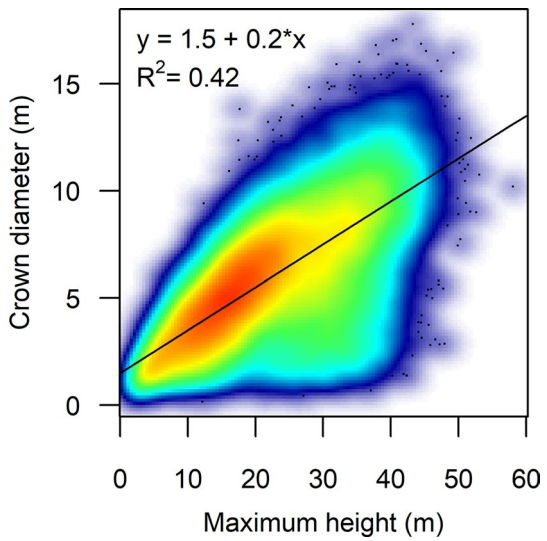

Fig. 3 Relationship between maximum height and crown diameter for lidar-detected tree objects across the study area ($n = 46{,}444$). The best-fit linear model was used as the moving window size for detecting CHM maxima for tree top identification

The normalized point cloud was segmented into individual tree objects by implementing the algorithm of Silva et al. (2016), which required the CHM and tree top locations as input, within the 'segment_trees' function of the 'lidR' package. The algorithm of Silva et al. (2016) was developed in and therefore performs relatively well in open pine forests (Hastings et al. 2020) like the ponderosa pine forest in our study area. We evaluated the tree segmentation by comparing the segmented tree objects with matched field-observed trees within a geographic information system (GIS); for each field-observed tree that could be reliably matched with a lidar object, we assessed whether the field-observed tree was either (1) correctly segmented, (2) over-segmented, i.e., the tree was separated into two tree objects when there should only be one, or (3) under-segmented, i.e., multiple trees were incorrectly grouped as one tree object.

Lidar height and intensity metrics for individual tree objects were created with the 'crown_metrics' function of the 'lidR' package (Table 2). Metrics included the normalized branch-bole foliage ratio (nbbfr; Wing et al. 2015; Oblinger et al. 2022), defined as:

$$nbbfr = \frac{(\#ofreturnswithintensity > 25) - (\#ofreturnswithintensity < 25)}{Total\#ofreturns} \quad (2)$$

where returns with intensity values > 25 are associated with foliage and returns with intensity values < 25 are associated with branches/boles. The intensity threshold used to distinguish woody versus foliage components is lidar acquisition dependent, as Wing et al. (2015) used an intensity threshold value of 60, and Oblinger et al. (2022) found an inverse relationship between short-wave infrared (SWIR, 1550 nm) lidar intensity (reflectance) and foliage/woody components. We determined an intensity threshold value for this lidar acquisition by examining lidar intensity histograms of live trees and snags in a preliminary analysis. An intensity value of 25 was selected because it was (1) midway between live tree and snag distribution peaks and (2) where distribution inflection points occurred (Fig. 4).

To assist in distinguishing live trees with topkill from others, individual tree metrics included the creation of a height density profile from which top-most returns were identified based on the highest profile peak height (Fig. 5). This highest profile peak height was identified with the 'peakwindow' function of the 'cardidates' R package (Rolinski et al. 2007) and was found to correspond with the field-measured live heights of trees with topkill ($R^2 = 0.57$, RMSE = 5 m). Metrics based on returns greater than this highest profile peak height were created to aid with classification (Table 2). A two-dimensional representation of tree object crowns as viewed from nadir were

Table 2 Candidate lidar metric variable names and descriptions. Top-most returns are defined as those with heights > the highest profile peak height (hpph; Fig. 5). Only first returns > 2 m in height above ground were used for metric creation

Metric name	Description
npoint	Number of returns
psingle	Percent single returns
crwn_dia	Crown diameter
hmean	Mean return height
hmax	Maximum return height
hmin	Minimum return height
hsd	Standard deviation of return heights
hskew	Skewness of return heights
hkurt	Kurtosis of return heights
hpph	Highest profile peak height (Fig. 5)
nbbfr	Normalized branch-bole/foliage ratio (Eq. 2)
imean	Mean return intensity
imax	Maximum return intensity
imin	Minimum return intensity
isd	Standard deviation of return intensities
iskew	Skewness of return intensities
ikurt	Kurtosis of return intensities
psingle_top	Percent single top-most returns
nbbfr_top	Normalized branch-bole/foliage ratio of top-most returns (Eq. 2)
imean_top	Mean return intensity of top-most returns
imax_top	Maximum return intensity of top-most returns
imin_top	Minimum return intensity of top-most returns
isd_top	Standard deviation of top-most return intensities
iskew_top	Skewness of top-most return intensities
ikurt_top	Kurtosis of top-most return intensities
imean_ratio	Mean intensity of top-most returns / mean intensity of lower returns

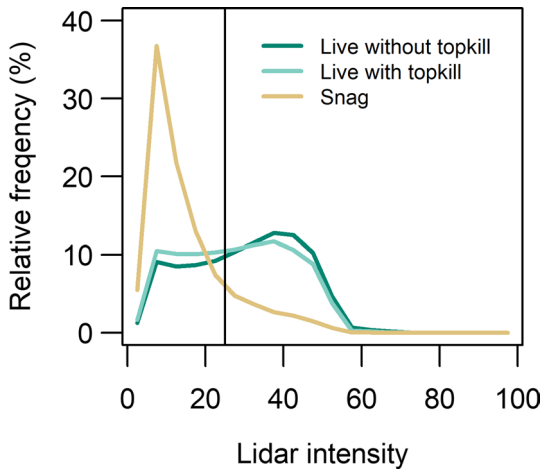

Fig. 4 Histograms of lidar return intensities for live trees, live trees with topkill, and snags. The vertical line represents a lidar intensity value of 25, which was selected to separate foliage and branch-bole returns

output as a polygon shapefile using the 'geom' = 'convex' switch of the 'crown_metrics' function in the lidR package. This polygon shapefile, which included crown metrics for each tree object, was used for model development and application.

Pairing field observations with lidar-detected tree objects

Field-measured tree locations, which included GNSS and field-measurement error, did not precisely overlay tree locations as represented by the CHM when visually assessed within a GIS. When apparent, field-measured tree locations were therefore adjusted within the GIS to correspond to the CHM and intersected with overlying tree crown polygons with the 'intersect' function of the 'terra' R package (Hijmans 2022). To maximize agreement between field-observed trees and lidar-detected tree objects, we calculated the three-dimensional (3D) Euclidean distance (Silva et al. 2016) between the two, defined as:

$$ed = \sqrt{(X_{\text{field}} - X_{\text{lidar}})^2 + (Y_{\text{field}} - Y_{\text{lidar}})^2 + (Z_{\text{field}} - Z_{\text{lidar}})^2} \quad (3)$$

where X_{field}, Y_{field}, Z_{field} are field-measured easting, northing, and tree height (m), respectively, and X_{lidar}, Y_{lidar}, Z_{lidar}

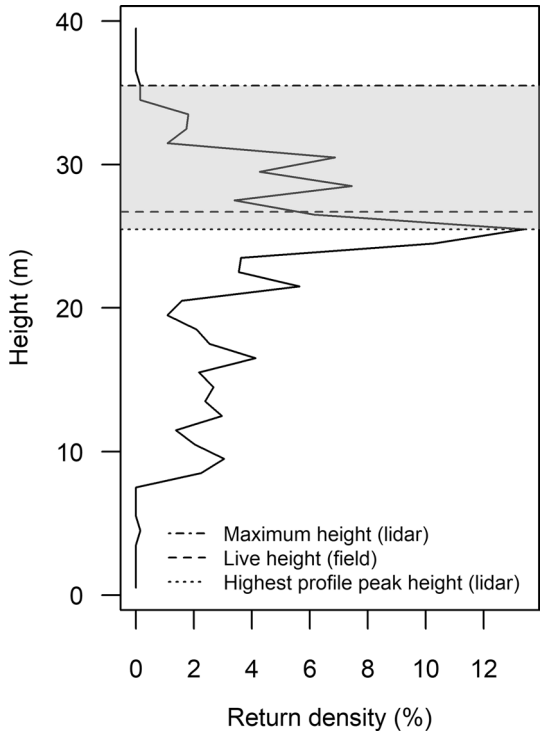

Fig. 5 Example of a lidar height density profile for a live tree with topkill. Maximum height, as measured by lidar, is shown as a dotted-and-dashed horizonal line. Live height, measured in the field, is represented by a dashed horizonal line. Highest profile peak height, determined from the 'peakwindow' function of the 'cardidates' R package (Rolinski et al. 2007), is represented by a dotted horizontal line. The gray area represents heights of returns that were used to create top-most return metrics

are lidar-measured easting, northing, and tree height (m), respectively. In cases where the polygon shapefile intersected more than one-field measured tree, we kept the pair with the smallest 3D Euclidean distance. We also dropped pairs where the 3D Euclidean distance was > 5 m. This resulted in 647 field-observed/lidar pairs. Of these, 524 (81.0%), 50 (7.7%), and 73 (11.3%) were identified in the field as live trees without topkill, live trees with topkill, and snags, respectively.

Random forest classification

We developed a random forest (RF) model (Breiman 2001) classifying lidar-derived tree objects as either live, live with topkill, or snag. Candidate predictor variables were the lidar metrics in Table 2. We implemented RF modeling in the 'randomForest' R package (Liaw and Wiener 2002) with 'ntree' and 'mtry' parameters of 500 and 3, respectively. Several iterations of the 'rf.modelSel' routine of the 'rfUtilities' R package were used to identify the most important variables and select the most parsimonious model (Murphy et al. 2010; Evans and Murphy 2018). For each 'rf.modelSel' iteration, we (1) randomly selected 73 of the 524 possible live tree samples for modeling, to balance classes (Chen et al. 2004; Shearman et al. 2019), and (2) included only one metric of highly correlated metric pairs, so that correlation did not influence predictor variable selection (Strobl et al. 2008). We chose a final RF model that minimized the out-of-bag (OOB) error rate with the fewest, uncorrelated ($R < 0.9$) predictor variables.

Table 3 Confusion matrix showing classification accuracy of trees as either live without topkill, live with topkill, or snag. Overall accuracy = 87%. $n = 196$ trees

Classification	Reference			Total	User acc. (%)
	No topkill	Topkill	Snag		
No topkill	68	9	2	79	86
Topkill	4	35	4	43	81
Snag	1	6	67	74	91
Total	73	50	73	196	
Prod. acc. (%)	93	70	92		Overall acc. = 87%

Tree crown map analysis

The final RF model was applied to all the lidar-detected tree crown objects using the 'predict' function of the 'terra' R package, to map tree crown status across the study area. Tree density grids were created by summarizing tree counts within 30-m grid cells across the study area to prioritize further field surveys and specific habitat evaluations.

Results

Field observations and classification accuracy

The overall mean dbh and height of trees at the plot-level was 55.5 cm (range 48.9–65.1) and 29.0 m (range 26.4–35.6), respectively. In plots, the primary causes of ponderosa pine mortality were attributed to fire and bark beetles (*Dendroctonus* and *Ips* spp.), while the main cause of topkill observed on ponderosa pine was comandra blister rust and to a lesser extent, bark beetles. The final RF model classified trees as either live, live with topkill, or snag with an overall accuracy of 87% (Table 3). Live tree with topkill was the most confused class and was equally confused between the live and snag classes. Live and snag classes were classified with similar high accuracies, having user and producer accuracies ranging from 86 to 93%.

Important predictor variables

Lidar intensity variables were consistently chosen as most important predictors, including intensity variables of the top-most returns (Fig. 6). The percent single returns, as well as the percent top-most single returns, were also particularly important. Height metrics helped increase classification accuracy but were the least important; when only height metrics were included, overall classification accuracy decreased to 74%. The normalized branch-bole/foliage ratio (nbbfr) and normalized branch-bole/foliage ratio of top-most returns (nbbfr_top) were frequently selected as the most important predictors but were also highly correlated with mean intensity and mean intensity of top-most returns ($R = 0.98–0.99$) and were therefore excluded in the final model.

Intensity metrics followed expected patterns, with snags being associated with lower and more varied intensity distributions (Fig. 7). Live trees were associated with greater percentages of single returns and snags with lower percentages of single returns, with top-killed trees being intermediate.

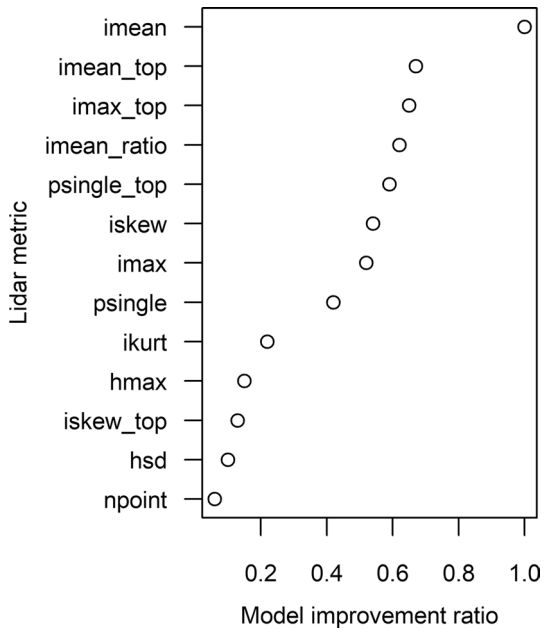

Fig. 6 Variable importance of selected predictor variables. The model improvement ratio is a normalized measure of variable importance, where 0 indicates least important, and 1 indicates most important. 'imean' = mean return intensity; 'imean_top' = mean return intensity of top-most returns; 'imax_top' = maximum return intensity of top-most returns; 'imean_ratio' = mean intensity of top-most returns / mean intensity of lower returns; 'psingle_top' = percent single top-most returns; 'iskew' = skewness of return intensities; 'imax' = maximum return intensity; 'psingle' = percent single returns; 'ikurt' = kurtosis of return intensities; 'hmax' = maximum return height; 'iskew_top' = skewness of top-most return intensities; 'hsd' = standard deviation of return heights; 'npoint' = number of returns

The ratio of the mean intensity of top-most returns to the mean intensity of lower returns (imean_ratio) was smallest for top-killed trees, as expected.

Tree health maps

Of the 647 field-observed/lidar-object tree pairs, we estimated that 90% were segmented correctly, 6% were over-segmented, and 4% were under-segmented, suggesting that our procedure for optimizing tree segmentation parameters successfully balanced inevitable under- and over-segmentation. A total of 46,444 tree objects were detected across the study area. Of these, 20,176 (43%) were classified as live, 10,184 (22%) were classified as having topkill, and 16,084 (35%) were classified as snags (Fig. 8). Tree density of 30-m grid cells across the study area averaged 204, 88, 45, and 71 ind. ha^{-1} for all live without topkill, live with topkill, and snag classes, respectively (Table 4). Tree density of all classes was spread evenly across densities of approximately 100 – 300 ind. ha^{-1}, with a peak around 200 ind. ha^{-1} (Fig. 9). The distribution of live tree density was concentrated around the mean of 88 ind. ha^{-1}, with many grid cells having live tree densities between 100 and 200 ha^{-1}. About 40% of grid cells contained < 25 ind. ha^{-1} of top-killed trees, with most cells containing < 100 top-killed ind. ha^{-1}, and a small number of cells containing high densities of > 100 top-killed ind. ha^{-1}. Snag density followed a positively skewed distribution like that of top-killed tree density. Snags were concentrated in recently burned areas (Fig. 10). Areas of high topkill density generally coincided with areas with higher live tree density. Topkill density was also relatively higher in the southern half of the study area.

Discussion

We provided another demonstration of mapping individual tree health by segmenting and classifying individual tree objects from airborne lidar data. Our overall classification accuracy of 87% is similar to accuracies of previous studies employing airborne lidar to classify individual live and dead tree objects (Appendix Table 5). Previous studies demonstrated the utility of lidar intensity metrics for distinguishing between live and dead tree biomass (Kim et al. 2009), predicting live and dead tree basal area (Bright et al. 2013), and identifying individual snags (Wing et al. 2015). Like others, we found that lidar intensity metrics, which describe the amount of laser energy reflected to the lidar sensor, were effective in distinguishing live and dead trees, with dead tree components being associated with lower near infrared (NIR) return intensities and live tree components being associated with higher NIR return intensities. Like previous studies, we developed a site-specific supervised classification; our

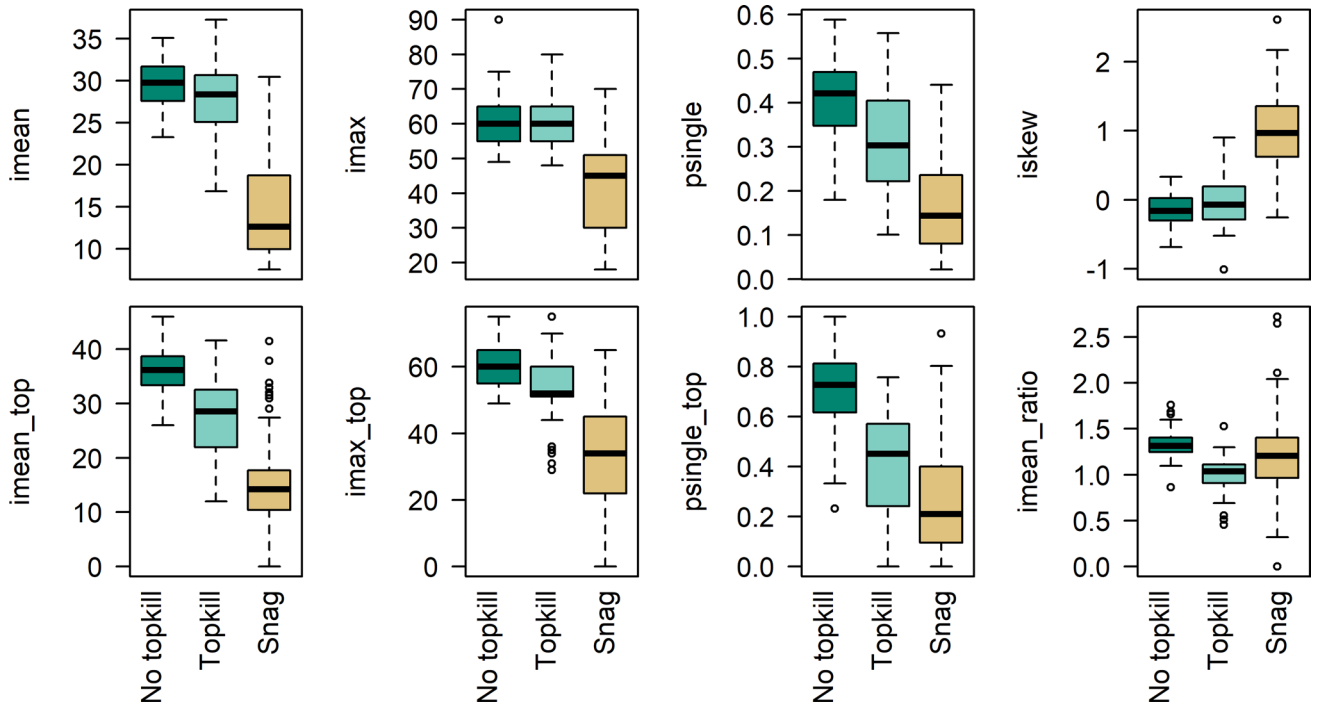

Fig. 7 Distributions (standard box plots) of most important selected metrics by tree class. 'imean' = mean return intensity; 'imean_top' = mean return intensity of top-most returns; 'imax' = maximum return intensity; 'imax_top' = maximum return intensity of top-most returns; 'psingle' = percent single returns; 'psingle_top' = percent single top-most returns; 'iskew' = skewness of return intensities; 'imean_ratio' = mean intensity of top-most returns / mean intensity of lower returns

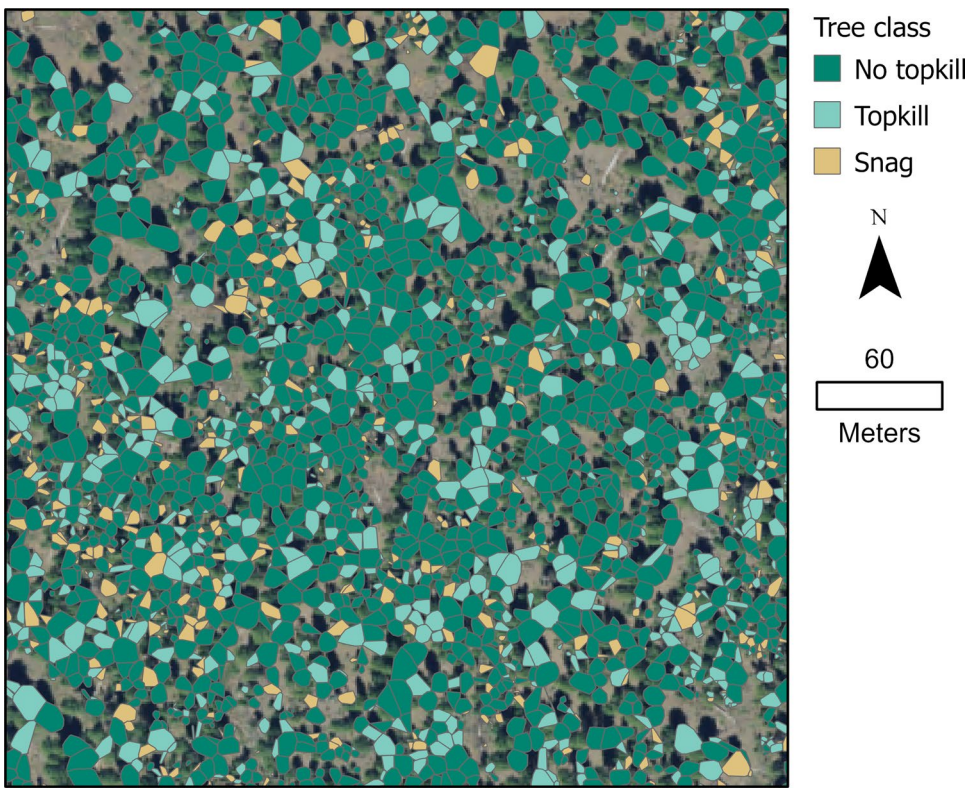

Fig. 8 Portion of the tree class map derived from applying the random forest model to all detected tree objects across the study area

Table 4 Tree density (ind. ha^{-1}) statistics of 30-m grid cells across the study area

Class	Minimum	Mean	Maximum	Standard deviation
All	0	204	778	98
No topkill	0	88	289	50
Topkill	0	45	456	40
Snag	0	71	478	79

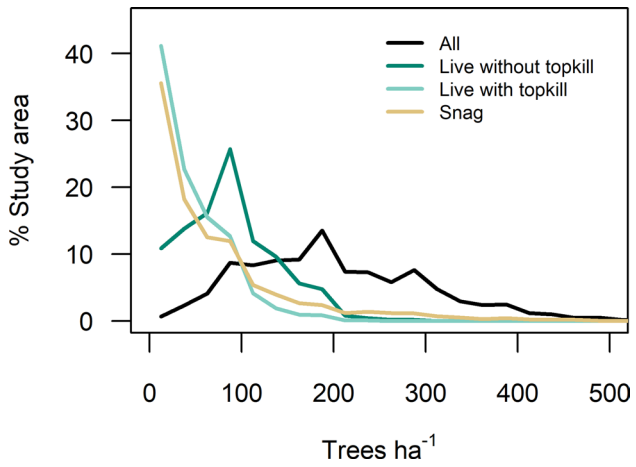

Fig. 9 Histograms of tree density (ind. ha^{-1}) by tree class for 30-m grid cells across the study area

methodology could be implemented in other conifer forests where airborne lidar data are available, however, a new classifier would need to be developed, especially since our classifier relied upon uncalibrated intensity data, which varies between lidar acquisitions. Care must be taken when using uncalibrated intensity measurements for analysis; generating rasters based on lidar intensity values and inspecting them for artifacts, as we did, is a simple method that can be used to determine whether lidar intensity information is fit for analysis. In our case, we benefited from the vendor being able to deliver lidar data where the influence of AGC on intensity values was removed. We also benefited from having a small study area with little topographic variation, so that the influence of range variation (distance of the terrain from the lidar sensor) on lidar intensity values was minimized.

We relied solely upon airborne lidar data for classification, which could be advantageous for others wishing to apply this methodology, as it does not rely upon multispectral data. Many previous studies found that the inclusion of multispectral or hyperspectral image variables improved accuracies, albeit less so if lidar intensity metrics are employed (Bright et al. 2013). Although many previous studies have demonstrated approaches which can successfully distinguish multiple classes or continuous measures of tree health (Appendix Table 5), to our knowledge, this is the first study demonstrating the separation of live, top-killed, and dead trees solely with airborne lidar data. In this study, intensity metrics were the most important predictors and served to explain much of the variation that likely would otherwise have been explained by multispectral or hyperspectral imagery. Our classification accuracies are similar to those of Shrestha et al. (2024), the only other study that we are aware of that has used point cloud data to detect top-killed conifers. They generated point clouds from multispectral drone imagery and used height and spectral data of point clouds to classify individual trees into six damage classes with an overall accuracy of 70%, as well as measure topkill height of damaged trees.

This study provides methods to help monitor effects of overlapping disturbances and further characterize structural diversity in forests. There are often multiple disturbance agents contributing to structural complexity at various scales in forest ecosystems (Agne et al. 2014; Hart and Kleinman 2018; Filip and Goheen 1982). In addition to fire as a major disturbance in forests of western North America, it is common for drought, insects and pathogens to alter stand and forest structure (Lalande et al. 2020; Reed et al. 2023; Spies et al. 2006). To conserve the diversity of old-growth characteristics in ponderosa pine and other forests prone to disturbance, estimates of structural elements are needed to help inform management decisions (Franklin and Van Pelt 2004; Spies et al. 2006). If live trees with topkill were not included in our assessment and the study area was evaluated only for snag presence, the total amount of dead wood and total structural elements available for wildlife habitat (e.g. either for cavity excavation or as perch sites for flycatchers and/or avian predators) would have been significantly underestimated.

Estimates of stand and snag densities, and the abundance of trees with topkill, could be evaluated in Oregon when considering a range of habitats in ponderosa pine. These estimates are likely to benefit our ability to identify suitable habitat for several wildlife species of greatest conservation need in Oregon (i.e. Strategy Species), many of whom would benefit from topkill either as important foraging perches and/or cavity excavation sites. Olive-sided flycatchers and Lewis's woodpeckers are listed in the top 5 Wildlife Priority Strategy Species List in various regions throughout Oregon (Oregon Department of Fish and Wildlife 2016), and both species that would benefit from topkill as it relates to increased foraging habitat that includes perch sites adjacent to areas in which these species can flycatch. Additionally, multiple woodpecker species are among the 58 avian Strategy Species, and those species include Lewis's woodpeckers, White-headed woodpeckers (*Dryobates albolarvatus*), and Pileated woodpeckers (*Dryocopus pileatus*) (Oregon Department of Fish and Wildlife

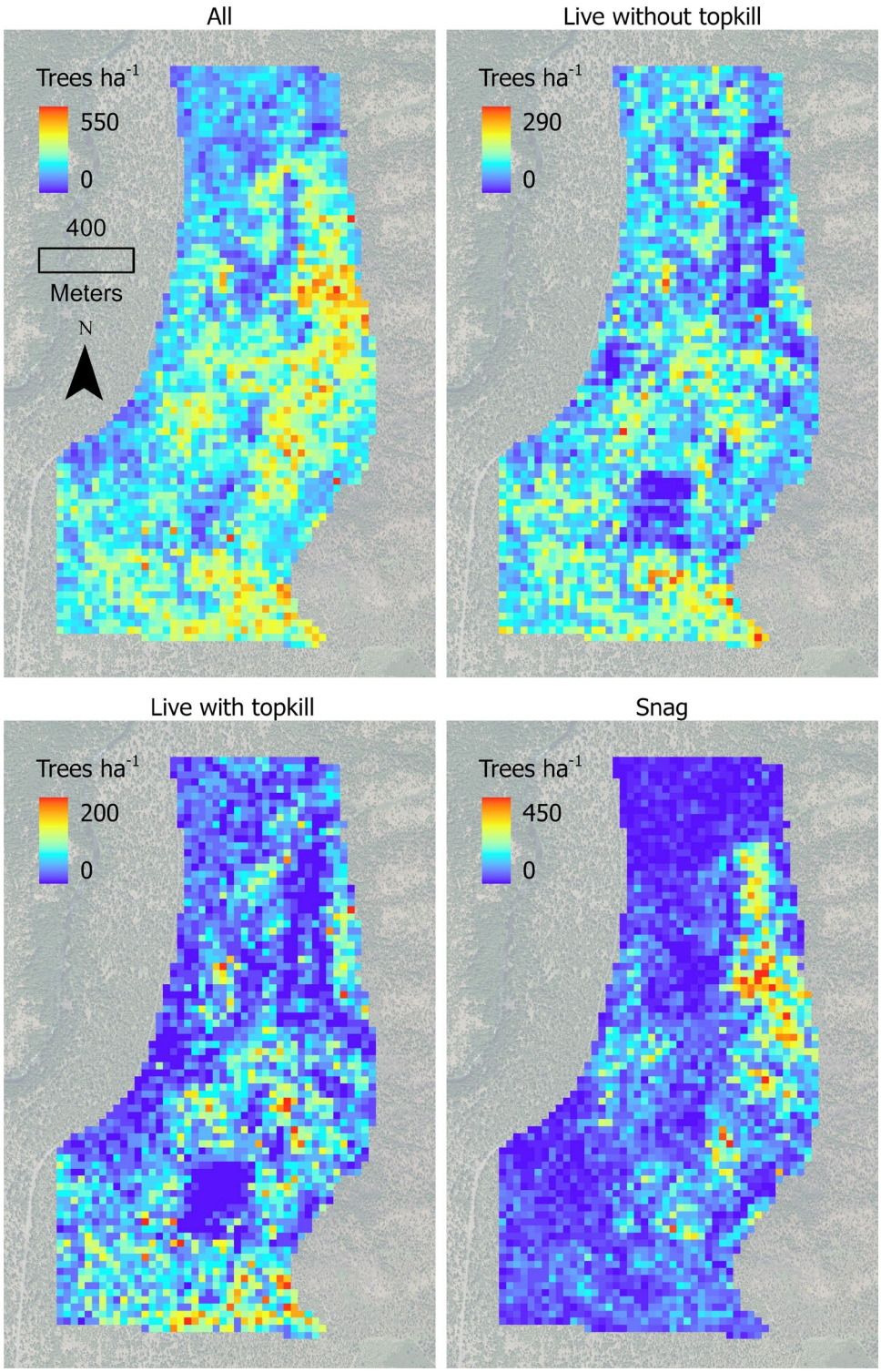

Fig. 10 Maps of tree density (ind. ha^{-1}) by tree class for 30-m grid cells across the study area

2016). The benefit of topkill to these different species is likely to vary because of species-specific selection for nest-site characteristics (e.g. wood characteristics at the site of excavation, diameter of topkill area, height off the ground, and surrounding vegetation characteristics). For instance, white-headed woodpeckers generally excavate tree cavities closer to the ground than many woodpecker species (Kozma et al. 2020) so might not use trees with topkill as much as a species like Lewis's woodpeckers (Vierling et al. 2020). Regardless of the initial source of excavated cavities though, excavated cavities can benefit

Table 5 Examples of studies in which airborne lidar or imagery-derived point data were used to classify the health of individual trees

References	Forest type(s)	Location	Tree classes (#)	Classification accuracy (%)
Yao et al. (2012)	Spruce, beech, maple	Germany	Live, dead (2)	73
Wing et al. (2015)	Pine, fir, mixed conifer	California, USA	Snag (1)	43–100 (detection rate)
Polewski et al. (2015)	Spruce, beech	Germany	Live, dead (2)	89
Casas et al. (2016)	Mixed conifer	California, USA	Live, dead (2)	92
Shendryk et al. (2016)	Eucalypt	Australia	Crown dieback and transparency (continuous)	81 (dieback) 70 (transparency)
Barnes et al. (2017)	Larch	Wales, United Kingdom	disease severity categories: not infected, infected (2) not infected, light, moderate, heavy (4)	72 (2 classes) 65 (4 classes)
Kamińska et al. (2018)	Spruce, pine and deciduous	Poland	Spruce, pine, deciduous, dead spruce, dead pine, dead deciduous (6)	94
Meng et al. (2018)	Mixed oak-pine	New York, USA	Canopy defoliation (continuous)	81
Lin et al. (2019)	Pine	China	Shoot damaged ratio (continuous)	83
Van Navarro-Cerrillo et al (2021)	Oak	Spain	Low, high defoliation (2)	87
*Cardil et al. (2019)	Pine-oak	Spain	No, low, high defoliation (3)	82–87
Krzystek et al. (2020)	Spruce, beech, fir, larch	Germany	Live, dead (2)	>90
Briechle et al. (2020)	Pine, birch, alder	Ukraine	Pine, birch, alder, dead (4)	90
Miltiadou et al. (2020)	Eucalypt	Australia	Dead (1)	72 (recall) 22 (precision)
Iversen (2020)	Spruce	Norway	Healthy, root rot infected (2)	63
Chi et al. (2020)	Urban (maple, horse chestnut, linden)	Belgium	Damage score (3)	81–89
*Abdollahnejad and Panagiotidis (2020)	Spruce, pine	Czech Republic	Healthy, unhealthy, dead (3)	85
Varo-Martínez and Navarro-Cerrillo (2021)	Pine	Spain	Slight, moderate, severe defoliation (3)	84
Yu et al. (2021)	Pine	China	Pine wilt disease infection stages: green, early, middle, heavy, and grey (5)	74
*Cessna et al. (2021)	Spruce	Alaska, USA	Non-infested, infested, dead (3)	78
Zhou et al. (2022)	Ash	China	Emerald ash borer infestation stages: healthy, light, moderate, severe (4)	83
Oblinger et al. (2022)	Fir	Oregon, USA	Live, dead (2) Healthy, unhealthy, recently-killed, dead (4)	95 (2 classes) 83 (4 classes)
Lin et al. (2023)	Pine	China	Crown damage (4)	78
*Shrestha et al. (2024)	Fir, pine, Douglas-fir	Montana, USA	Healthy, damaged (2) Healthy, damage level, dead (6)	94 (2 classes) 70 (6 classes)
Oblinger et al. (this study) (2026)	Pine	Oregon, USA	Live, top-killed, dead (3)	87

*Point cloud data generated photogrammetrically from multispectral imagery, references above are included in the list of References

multiple species across seasons and years (e.g. Gentry and Vierling 2008; Edworthy et al. 2018; Cadieux et al. 2023).

"Spike tops", caused by comandra blister rust, were commonly observed in mature ponderosa pine throughout the study area and field observations indicated that some large, old ponderosa pines can persist living for many decades with topkill enhancing structural diversity at this location reported by Filip (1977). However, it is likely that some live

trees with topkill have died since Filip (1977) documented living pines with topkill here. We found more trees with topkill in the southern half of the study area that coincided with where Filip (1977) reported more topkill in some plots. Wave years happen where more comandra blister rust infections occur (Jacobi et al. 2002), and Filip (1977) suggested that numerous infections likely occurred sometime around 1936 at this location. Overall, we detected a higher incidence of topkill in 2016 across the study area than Filip (1977) using different methods. We detected an overall mean density of live trees with topkill that was over four times the mean density that Filip (1977) found, which suggests topkill on live individuals has increased over the last 40 years since 1976. A recent increase in comandra blister rust, and other stem rusts of hard pines, has been associated with a changing climate in British Columbia (Woods 2014; Hennon et al. 2021). The higher frequency of wave years when more infections are occurring there appears to be associated with changes in precipitation and warmer overnight temperatures. The need for additional monitoring of stem rusts has been identified under a changing climate (Hennon et al. 2021), along with possible changes in other disturbance regimes, and our approach could aid in the detection and monitoring of damage due to stem rusts elsewhere.

Topkill on *Pinus contorta* can also occur due to western gall rust bole infections, caused by the fungus *Cronartium harknessii*, and other stem rusts (Dahms 1965; Mulvey and Bisbing 2016). Topkill and tree mortality often results from stem girdling cankers on five-needle pines due to the non-native disease white pine blister rust, caused by *Cronartium ribicola*, in North America (Geils et al. 2010). Additional methods for monitoring damage in ecologically important five-needle pines, such as whitebark pine (*Pinus albicaulis*), threatened by *Cronartium ribicola* are needed going forward (Tomback and Sprague 2022). Topkill is not always visible to observers in fixed-wing aircraft during forest health aerial surveys and is inconsistently recorded, or in some cases, mistaken for tree mortality (Ciesla 2006; Coleman et al. 2018). Therefore, having other methods to detect topkill is needed, and our approach could be used to prioritize areas for field surveys to further refine estimates of topkill versus tree mortality.

Our approach could be applied to improve detection of topkill, along with tree mortality, in conifers caused by a number of disturbances. Topkill is common on trees that become severely infected with dwarf mistletoe (*Arceuthobium* sp.) (Mathiasen et al. 2008). Topkill is commonly associated with insect damage caused by some defoliators and *Scolytus* engraver beetles (Furniss and Carolin 1977; Ciesla 2006). Pine defoliation due to the jack pine budworm (*Choristoneura pinus*) and pine looper (*Bupalus piniaria*) can result in topkill and tree mortality (Volney 1998; Cedervind and Långström 2003). Topkill in Douglas-fir and true firs (*Abies* spp.) is often observed following defoliation by the western spruce budworm (*Choristoneura freemani*) and Douglas-fir tussock moth (*Orgyia pseudotsugata*) (Wickman 1978; Aho 1984; Alfaro et al. 1987).

The amount of crown damage reducing leaf area in conifers influences a tree's physiologic function, growth and the risk of tree mortality (Miller and Keen 1960; Ferrell 1980; Sheppard and Ford 1986; Geils and Jacobi 1993). Geils and Jacobi (1993) reported significant reductions in growth and survival of lodgepole pine with topkill caused by comandra blister rust. As crown loss became severe, a greater reduction in radial growth and survival was observed. Miller and Keen (1960) noted examples of ponderosa pine in Oregon and California with topkill being predisposed to mortality by western pine beetle (*Dendroctonus brevicomis*). True firs (*Abies* spp.) with severe topkill due to repeated damage by balsam woolly adelgid (*Adelges piceae*) in Oregon and Washington often die (Mitchell and Buffam 2001). Topkilled true firs associated with Douglas-fir tussock moth damage may be predisposed to mortality by bark beetles (Wickman 1963; 1978). Merchantability of conifers with topkill is also reduced compared to trees without topkill, and remote detection of topkill could improve estimates of timber volume (Childs 1968; Ferrell and Scharpf 1982; Hall et al. 1993).

Conclusion

This study provides a novel approach for using airborne lidar to distinguish individual conifers with topkill, live conifers without topkill and snags. During management planning, estimates of the occurrence of individual trees with topkill, in addition to snags, would be useful to wildlife biologists, silviculturists and other forest resource managers when considering the impacts of treatment alternatives and wildlife habitat availability. The overall health of crowns and live crown ratio of conifers is typically correlated with growth and vigor of individual trees; thus, our approach can be utilized to improve detection of damage and stress in live trees to further evaluate forest health conditions. Retention of large, living trees is often a restoration treatment objective, and our methods could be used to target areas for stand density reduction treatments to maintain large, living trees with topkill (Kolb et al. 2007; McDowell et al. 2003). During vegetation management planning around developed recreation sites and along frequently used roads, identifying locations with dead trees and live trees with topkill posing a hazard to public safety, due to the risk of stem breakage, would also help to prioritize ground surveys and hazard mitigation activities (Terho et al. 2007). Further studies utilizing airborne lidar combined with additional remotely sensed data, such as multispectral imagery, are encouraged for improved

detection of live trees with topkill differentiated from live trees without topkill and snags, especially when reliable lidar intensity values may be unavailable.

Declarations

Conflict of interest The authors declare that they have no conflict of interest.

Appendix

See Table 5.

References

Abdollahnejad A, Panagiotidis D (2020) Tree species classification and health status assessment for a mixed broadleaf-conifer forest with UAS multispectral imaging. Remote Sens 12(22):3722. https://doi.org/10.3390/rs12223722

Agne MC, Shaw DC, Woolley TJ, Queijeiro-Bolaños ME (2014) Effects of dwarf mistletoe on stand structure of lodgepole pine forests 21–28 years post-mountain pine beetle epidemic in central Oregon. PLoS ONE 9(9):e107532. https://doi.org/10.1371/journal.pone.0107532

Aho PE (1984) Losses associated with Douglas-fir and true fir tops killed by western spruce budworm in eastern Washington. USDA Forest Service, Pacific Northwest Forest and Range Experiment Station, Portland, OR. https://doi.org/10.2737/PNW-RP-318

Alfaro RI, Wegwitz E, Brown RG, Taylor SP (1987) Douglas-fir tussock moth damage in British Columbia. For Chron 63(5):351–355. https://doi.org/10.5558/tfc63351-5

Altman B, Sallabanks R (2020) Olive-sided flycatcher (Contopus cooperi), version 10. In: Poole AF (ed) Birds of the world. Cornell Lab of Ornithology, Ithaca, NY, USA. https://doi.org/10.2173/bow.olsfly.01

Barnes C, Balzter H, Barrett K, Eddy J, Milner S, Suárez JC (2017) Airborne laser scanning and tree crown fragmentation metrics for the assessment of *Phytophthora ramorum* infected larch forest stands. For Ecol Manage 404:294–305. https://doi.org/10.1016/j.foreco.2017.08.052

Bell DM, Acker SA, Gregory MJ, Davis RJ, Garcia BA (2021) Quantifying regional trends in large live tree and snag availability in support of forest management. For Ecol Manage 479:118554. https://doi.org/10.1016/j.foreco.2020.118554

Bergdahl DR, French DW (1976) Epidemiology of comandra rust on jack pine and comandra in Minnesota. Can J for Res 6(3):326–334. https://doi.org/10.1139/x76-043

Breiman L (2001) Random forests. Mach Learn 45(1):5–32. https://doi.org/10.1023/A:1010933404324

Briechle S, Krzystek P, Vosselman G (2020) Classification of tree species and standing dead trees by fusing UAV-based lidar data and multispectral imagery in the 3D deep neural network PointNet++. ISPRS Ann Photogramm Remote Sens Spatial Inf Sci. https://doi.org/10.5194/isprs-annals-V-2-2020-203-2020

Bright BC, Hudak AT, McGaughey R, Andersen HE, Negrón J (2013) Predicting live and dead tree basal area of bark beetle affected forests from discrete-return lidar. Can J Remote Sens 39(Sup1):S99–S111. https://doi.org/10.5589/m13-027

Bunnell FL (2013) Sustaining cavity-using species: patterns of cavity use and implications to forest management. ISRN for 2013(1):457698. https://doi.org/10.1155/2013/457698

Cadieux P, Drapeau P, Ouellet-Lapointe U, Leduc A, Imbeau L, Deschênes R, Nappi A (2023) Old forest structural development drives complexity of nest webs in a naturally disturbed boreal mixedwood forest landscape. Front for Glob Change 6:1084696. https://doi.org/10.3389/ffgc.2023.1084696

Cardil A, Otsu K, Pla M, Silva CA, Brotons L (2019) Quantifying pine processionary moth defoliation in a pine-oak mixed forest using unmanned aerial systems and multispectral imagery. PLoS ONE 14(3):e0213027. https://doi.org/10.1371/journal.pone.0213027

Casas Á, García M, Siegel RB, Koltunov A, Ramírez C, Ustin S (2016) Burned forest characterization at single-tree level with airborne laser scanning for assessing wildlife habitat. Remote Sens Environ 175:231–241. https://doi.org/10.1016/j.rse.2015.12.044

Cedervind J, Långström B (2003) Tree mortality, foliage recovery and top-kill in stands of Scots pine (*Pinus sylvestris*) subsequent to defoliation by the pine looper (*Bupalus piniaria*). Scand J Res 18(6):505–513. https://doi.org/10.1080/02827580310018569

Cessna J, Alonzo MG, Foster AC, Cook BD (2021) Mapping boreal forest spruce beetle health status at the individual crown scale using fused spectral and structural data. Forests 12(9):1145. https://doi.org/10.3390/f12091145

Chen C, Liaw A, Breiman L (2004) Using random forest to learn imbalanced data. University of California, Berkeley. https://statistics.berkeley.edu/sites/default/files/tech-reports/666.pdf [Accessed on 30.10.2024]

Chi DK, Degerickx J, Yu K, Somers B (2020) Urban tree health classification across tree species by combining airborne laser scanning and imaging spectroscopy. Remote Sens 12(15):2435. https://doi.org/10.3390/rs12152435

Childs TW (1968) Comandra rust damage to ponderosa pine in Oregon and Washington. USDA Forest Service, Pacific Northwest Forest and Range Experiment Station, Portland, OR

Ciesla WM (2006) Describing signatures: a key to successful use of remote sensing for forest damage assessment. Ambiência 2(3):153–167. https://revistas.unicentro.br/index.php/ambiencia/article/view/264 [accessed on 30.10.2024]

Coleman TW, Graves AD, Heath Z, Flowers RW, Hanavan RP, Cluck DR, Ryerson D (2018) Accuracy of aerial detection surveys for mapping insect and disease disturbances in the United States. For Ecol Manage 430:321–336. https://doi.org/10.1016/j.foreco.2018.08.020

Dahms WG (1965) Rust cankers: a threat to central Oregon lodgepole pine? USDA Forest Service, Pacific Northwest Forest and Range Experiment Station, Portland, OR

Dolph KL, Mori SR, Oliver WW (1995) Long-term response of old-growth stands to varying levels of partial cutting in the eastside pine type. West j Appl for 10(3):101–108. https://doi.org/10.1093/wjaf/10.3.101

Edworthy AB, Trzcinski MK, Cockle KL, Wiebe KL, Martin K (2018) Tree cavity occupancy by nesting vertebrates across cavity age. J Wildl Manage 82(3):639–648. https://doi.org/10.1002/jwmg.21398

Evans JS, Murphy MA (2018) rfUtilities. R package version 2.1–3. https://cran.r-project.org/web/packages/rfUtilities/index.html [Accessed on 30.10.2024]

Ferrell GT, Scharpf RF (1982) Stem volume losses in grand firs top-killed by western spruce budworm in Idaho. USDA Forest Service, Pacific Southwest Forest and Range Experiment Station, Berkeley, CA. https://doi.org/10.2737/PSW-RP-164

Ferrell GT (1980) Risk-rating systems for mature red fir and white fir in northern California. USDA Forest Service, Pacific Southwest Forest and Range Experiment Station, Berkeley, CA. https://doi.org/10.2737/PSW-GTR-39

Fiedler CE, Friederici P, Petruncio M (2007) Monitoring old growth in frequent-fire landscapes. Ecol Society 12(2):22. http://www.ecologyandsociety.org/vol12/iss2/art22/ [accessed on 30.10.2024]

Filip GM (1977) Crown mortality of ponderosa pine caused by *Cronartium comandrae*. Plant Dis Report 61:1083–1085

Filip GM, Goheen DJ (1982) Tree mortality caused by root pathogen complex in Deschutes National Forest, Oregon. Plant Dis 66(1):240–243. https://doi.org/10.1094/pd-66-240

Franklin JF, Van Pelt R (2004) Spatial aspects of structural complexity in old-growth forests. J for 102(3):22–28. https://doi.org/10.1093/jof/102.3.22

Froidevaux JSP, Zellweger F, Bollmann K, Jones G, Obrist MK (2016) From field surveys to LiDAR: shining a light on how bats respond to forest structure. Remote Sens Environ 175:242–250. https://doi.org/10.1016/j.rse.2015.12.038

Furniss RL, Carolin VM (1977) Western forest insects (No. 1339). USDA Forest Service, Washington, DC

Geils BW, Jacobi WR (1990) Development of comandra blister rust on lodgepole pine. Can J for Res 20(2):159–165. https://doi.org/10.1139/x90-022

Geils BW, Jacobi WR (1993) Effects of comandra blister rust on growth and survival of lodgepole pine. Phytopathology 83(6):638–644. https://doi.org/10.1094/phyto-83-638

Geils BW, Hummer KE, Hunt RS (2010) White pines, *Ribes*, and blister rust: a review and synthesis. For Pathol 40(3–4):147–185. https://doi.org/10.1111/j.1439-0329.2010.00654.x

Gentry DJ, Vierling KT (2008) Reuse of woodpecker cavities in the breeding and non-breeding seasons in old burn habitats in the Black Hills, South Dakota. Am Midl Nat 160:413–429. https://doi.org/10.1674/0003-0031(2008)160[413:ROWCIT]2.0.CO;2

Hagmann RK, Franklin JF, Johnson KN (2013) Historical structure and composition of ponderosa pine and mixed-conifer forests in south-central Oregon. For Ecol Manag 304:492–504. https://doi.org/10.1016/j.foreco.2013.04.005

Hall RJ, Titus SJ, Volney WJA (1993) Estimating top-kill volumes with large-scale photos on trees defoliated by the jack pine budworm. Can J for Res 23(7):1337–1346. https://doi.org/10.1139/x93-171

Hardin FO, Leivers S, Grace JK, Hancock Z, Campbell T, Pierce B, Morrison ML (2021) Secondhand homes: the multilayered influence of woodpeckers as ecosystem engineers. Ecol Evol 11(16):11425–11439. https://doi.org/10.1002/ece3.7932

Harmon ME, Franklin JF, Swanson FJ, Sollins P, Gregory SV, Lattin JD, Anderson NH, Cline SP, Aumen NG, Sedell JR, Lienkaemper GW (2004) Ecology of coarse woody debris in temperate ecosystems. Adv Ecol Res 34:59–234. https://doi.org/10.1016/S0065-2504(08)60121-X

Harrod RJ, McRae BH, Hartl WE (1999) Historical stand reconstruction in ponderosa pine forests to guide silvicultural prescriptions. For Ecol Manag 114(2–3):433–446. https://doi.org/10.1016/S0378-1127(98)00373-9

Hart JL, Kleinman JS (2018) What are intermediate-severity forest disturbances and why are they important? Forests 9(9):579. https://doi.org/10.3390/f9090579

Hastings JH, Ollinger SV, Ouimette AP, Sanders-DeMott R, Palace MW, Ducey MJ, Sullivan FB, Basler D, Orwig DA (2020) Tree species traits determine the success of LiDAR-based crown mapping in a mixed temperate forest. Remote Sens 12(2):309. https://doi.org/10.3390/rs12020309

Hennon PE, Frankel SJ, Woods AJ, Worrall JJ, Ramsfield TD, Zambino PJ, Shaw DC, Ritóková G, Warwell MV, Norlander D, Mulvey RL, Shaw CG III (2021) Applications of a conceptual framework to assess climate controls of forest tree diseases. For Pathol 51(6):e12719. https://doi.org/10.1111/efp.12719

Hijmans R (2022) terra: Spatial Data Analysis. R package version 1.6–7. https://cran.r-project.org/web/packages/terra/index.html [accessed on 30.10.2024]

Isenbrg M (2020) LAStools: efficient LiDAR processing software (version 200216, academic). http://rapidlasso.com/LAStools [accessed on 30.10.2024]

Iversen EA (2020) Detection of root and butt rot in Norway Spruce (*Picea abies*) using airborne hyperspectral images and laser scanning. Dissertation, Norwegian University of Life Sciences, Ås.

Jacobi WR, Geils BW, Taylor JE (2002) Frequency of comandra blister rust infections on lodgepole pine. USDA Forest Service, Rocky Mountain Research Station, Fort Collins, CO. https://doi.org/10.2737/RMRS-RP-36

Jacobi WR (1993) Insects emerging from lodgepole pine infected with Comandra blister rust. USDA Forest Service, Rocky Mountain Research Station, Fort Collins, CO

Janisch JE, Harmon ME (2002) Successional changes in live and dead wood carbon stores: implications for net ecosystem productivity. Tree Physiol 22(2–3):77–89. https://doi.org/10.1093/treephys/22.2-3.77

Johnson DW (1979) Growth and development of comandra rust cankers on young lodgepole pine. Plant Dis Rep 63:916–918

Johnson DW (1986) Comandra blister rust. Forest Insect and Disease Leaflet 62, USDA Forest Service

Jung K, Kaiser S, Böhm S, Nieschulze J, Kalko EKV (2012) Moving in three dimensions: effects of structural complexity on occurrence and activity of insectivorous bats in managed forest stands. J Appl Ecol 49(2):523–531. https://doi.org/10.1111/j.1365-2664.2012.02116.x

Kamińska A, Lisiewicz M, Stereńczak K, Kraszewski B, Sadkowski R (2018) Species-related single dead tree detection using multi-temporal ALS data and CIR imagery. Remote Sens Environ 219:31–43. https://doi.org/10.1016/j.rse.2018.10.005

Kilgo JC, Vukovich MA (2014) Can snag creation benefit a primary cavity nester: response to an experimental pulse in snag abundance. Biol Conserv 171:21–28. https://doi.org/10.1016/j.biocon.2014.01.003

Kim Y, Yang ZQ, Cohen WB, Pflugmacher D, Lauver CL, Vankat JL (2009) Distinguishing between live and dead standing tree biomass on the North Rim of Grand Canyon National Park, USA using small-footprint lidar data. Remote Sens Environ 113(11):2499–2510. https://doi.org/10.1016/j.rse.2009.07.010

Kolb TE, Agee JK, Fulé PZ, McDowell NG, Pearson K, Sala A, Waring RH (2007) Perpetuating old ponderosa pine. For Ecol Manag 249(3):141–157. https://doi.org/10.1016/j.foreco.2007.06.002

Korpela I, Ørka HO, Hyyppä J, Heikkinen V, Tokola T (2010) Range and AGC normalization in airborne discrete-return LiDAR intensity data for forest canopies. ISPRS J Photogramm Remote Sens 65(4):369–379. https://doi.org/10.1016/j.isprsjprs.2010.04.003

Kozma JM, Lorenz TJ, Raphael MG, Garrett KL, Dixon RD (2020) White-headed woodpecker (Dryobates albolarvatus), version 20. In: Rodewald PG, Keeney BK (eds) Birds of the World. Cornell

Lab of Ornithology, Ithaca, NY. https://doi.org/10.2173/bow.whhwoo.02
Krzystek P, Serebryanyk A, Schnörr C, Červenka J, Heurich M (2020) Large-scale mapping of tree species and dead trees in Šumava National Park and Bavarian Forest National Park using lidar and multispectral imagery. Remote Sens 12(4):661. https://doi.org/10.3390/rs12040661
Lalande BM, Hughes K, Jacobi WR, Tinkham WT, Reich R, Stewart JE (2020) Subalpine fir mortality in Colorado is associated with stand density, warming climates and interactions among fungal diseases and the western balsam bark beetle. For Ecol Manage 466:118133. https://doi.org/10.1016/j.foreco.2020.118133
Liaw A, Wiener M (2002) Classification and regression by randomForest. R News, 2(3):18–22. https://journal.r-project.org/articles/RN-2002-022/RN-2002-022.pdf [accessed on 30.10.2024]
Lin QN, Huang HG, Wang JX, Huang K, Liu YY (2019) Detection of pine shoot beetle (PSB) stress on pine forests at individual tree level using UAV-based hyperspectral imagery and lidar. Remote Sens 11(21):2540. https://doi.org/10.3390/rs11212540
Lin QN, Huang HG, Wang JX, Chen L, Du HQ, Zhou GM (2023) Early detection of pine shoot beetle attack using vertical profile of plant traits through UAV-based hyperspectral, thermal, and lidar data fusion. Int J Appl Earth Obs Geoinf 125:103549. https://doi.org/10.1016/j.jag.2023.103549
Lutz JA, Struckman S, Germain SJ, Furniss TJ (2021) The importance of large-diameter trees to the creation of snag and deadwood biomass. Ecol Process 10(1):28. https://doi.org/10.1186/s13717-021-00299-0
Marcot BG, Ohmann JL, Mellen-McLean K, Waddell KL (2010) Synthesis of regional wildlife and vegetation field studies to guide management of standing and down dead trees. For Sci 56(4):391–404. https://doi.org/10.1093/forestscience/56.4.391
Mathiasen RL, Nickrent DL, Shaw DC, Watson DM (2008) Mistletoes: pathology, systematics, ecology, and management. Plant Dis 92(7):988–1006. https://doi.org/10.1094/PDIS-92-7-0988
McDowell N, Brooks JR, Fitzgerald SA, Bond BJ (2003) Carbon isotope discrimination and growth response of old *Pinus ponderosa* trees to stand density reductions. Plant Cell Environ 26(4):631–644. https://doi.org/10.1046/j.1365-3040.2003.00999.x
McGaughey RJ (2022) FUSION/LDV: software for lidar data analysis and visualization. USDA Forest Service, Pacific Northwest Research Station. https://forsys.sefs.uw.edu/fusion/fusionlatest.html [accessed on 30.10.2024]
Meddens AJH, Hicke JA, Vierling LA (2011) Evaluating the potential of multispectral imagery to map multiple stages of tree mortality. Remote Sens Environ 115(7):1632–1642. https://doi.org/10.1016/j.rse.2011.02.018
Meng R, Dennison PE, Zhao F, Shendryk I, Rickert A, Hanavan RP, Cook BD, Serbin SP (2018) Mapping canopy defoliation by herbivorous insects at the individual tree level using bi-temporal airborne imaging spectroscopy and LiDAR measurements. Remote Sens Environ 215:170–183. https://doi.org/10.1016/j.rse.2018.06.008
Mercer C, Comeau VM, Daniels LD, Carrer M (2022) Contrasting impacts of climate warming on coastal old-growth tree species reveal an early warning of forest decline. Front for Glob Change 4:775301. https://doi.org/10.3389/ffgc.2021.775301
Miller JM, Keen FP (1960) Biology and control of the western pine beetle. USDA Forest Service, Misc. Publication 800, Washington, DC
Miller DR, Blomstrom R (1968) Determining the age of comandra rust infection on ponderosa pine in California. Plant Dis Report 52:305–307
Miltiadou M, Agapiou A, Gonzalez Aracil S, Hadjimitsis DG (2020) Detecting dead standing eucalypt trees from voxelised full-waveform lidar using multi-scale 3D-windows for tackling height and size variations. Forests 11(2):161. https://doi.org/10.3390/f11020161
Mitchell RG, Buffam PE (2001) Patterns of long-term balsam woolly adelgid infestations and effects in Oregon and Washington. West j Appl for 16(3):121–126. https://doi.org/10.1093/wjaf/16.3.121
Monahan WB, Arnspiger CE, Bhatt P, An ZM, Krist FJ, Liu T, Richard RP, Edson C, Froese RE, Steffenson J, Lammers TC, Frosh R (2022) A spectral three-dimensional color space model of tree crown health. PLoS ONE 17(10):e0272360. https://doi.org/10.1371/journal.pone.0272360
Mulvey RL, Bisbing SM (2016) Complex interactions among agents affect shore pine health in southeast Alaska. Northwest Sci 90(2):176–194. https://doi.org/10.3955/046.090.0209
Murphy MA, Evans JS, Storfer A (2010) Quantifying *Bufo boreas* connectivity in Yellowstone National Park with landscape genetics. Ecology 91(1):252–261. https://doi.org/10.1890/08-0879.1
Oblinger BW, Bright BC, Hanavan RP, Simpson M, Hudak AT, Cook BD, Corp LA (2022) Identifying conifer mortality induced by *Armillaria* root disease using airborne lidar and orthoimagery in south central Oregon. For Ecol Manage 511:120126. https://doi.org/10.1016/j.foreco.2022.120126
Oregon Department of Fish and Wildlife (2016) The Oregon conservation strategy: Chapter 6: strategy species. https://oregonconservationstrategy.org/media/6-Strategy-Species-12.30.16.pdf [accessed on 30.10.2024]
Perrakis DDB, Agee JK, Eglitis A (2011) Effects of prescribed burning on mortality and resin defenses in old growth ponderosa pine (Crater Lake, Oregon): four years of post-fire monitoring. Nat Areas J 31(1):14–25. https://doi.org/10.3375/043.031.0103
Polewski P, Yao W, Heurich M, Krzystek P, Stilla U (2015) Active learning approach to detecting standing dead trees from ALS point clouds combined with aerial infrared imagery. In: 2015 IEEE Conference on Computer Vision and Pattern Recognition Workshops (CVPRW), Boston, MA, USA. pp 10–18. https://doi.org/10.1109/CVPRW.2015.7301378
Popescu S, Wynne R (2004) Seeing the trees in the forest: using lidar and multispectral data fusion with local filtering and variable window size for estimating tree height. Photogramm Eng Remote Sens 70(5):589–604. https://doi.org/10.14358/PERS.70.5.589
Powell JM (1970) *Cronartium comandrae* in Canada, its distribution and hosts. Can J Plant Pathol 50:130–135
R Core Team (2022) R: a language and environment for statistical computing. R Foundation for Statistical Computing, Vienna, Austria. https://www.R-project.org/ [accessed on 30.10.2024]
Raphael MG, White M (1984) Use of snags by cavity-nesting birds in the Sierra Nevada. Wildl Monogr 86:3–66
Reed CC, Hood SM, Cluck DR, Smith SL (2023) Fuels change quickly after California drought and bark beetle outbreaks with implications for potential fire behavior and emissions. Fire Ecol 19(1):16. https://doi.org/10.1186/s42408-023-00175-6
Rolinski S, Horn H, Petzoldt T, Paul L (2007) Identifying cardinal dates in phytoplankton time series to enable the analysis of long-term trends. Oecologia 153(4):997–1008. https://doi.org/10.1007/s00442-007-0783-2
Roussel JR, Auty D, Coops NC, Tompalski P, Goodbody TRH, Meador AS, Bourdon JF, de Boissieu F, Achim A (2020) lidR: an R package for analysis of Airborne Laser Scanning (ALS) data. Remote Sens Environ 251:112061. https://doi.org/10.1016/j.rse.2020.112061
Roussel JR, Auty D (2022) Airborne LiDAR data manipulation and visualization for forestry applications. R package version 4.0.1. https://cran.r-project.org/package=lidR [accessed on 30.10.2024]
Sánchez Meador AJ, Waring KM, Kalies EL (2015) Implications of diameter caps on multiple forest resource responses in the

context of the four forests restoration initiative: results from the forest vegetation simulator. J for 113(2):219–230. https://doi.org/10.5849/jof.14-021

Sandström J, Bernes C, Junninen K, Lõhmus A, Macdonald E, Müller J, Jonsson BG (2019) Impacts of dead wood manipulation on the biodiversity of temperate and boreal forests. A systematic review. J Appl Ecol 56(7):1770–1781. https://doi.org/10.1111/1365-2664.13395

Shearman TM, Varner JM, Hood SM, Cansler CA, Hiers JK (2019) Modelling post-fire tree mortality: can random forest improve discrimination of imbalanced data? Ecol Model 414:108855. https://doi.org/10.1016/j.ecolmodel.2019.108855

Shendryk I, Broich M, Tulbure MG, McGrath A, Keith D, Alexandrov SV (2016) Mapping individual tree health using full-waveform airborne laser scans and imaging spectroscopy: a case study for a floodplain eucalypt forest. Remote Sens Environ 187:202–217. https://doi.org/10.1016/j.rse.2016.10.014

Sheppard LJ, Ford ED (1986) Genetic and environmental control of crown development in *Picea sitchensis* and its relation to stem wood production. Tree Physiol 1(3):341–354. https://doi.org/10.1093/treephys/1.3.341

Shrestha A, Hicke JA, Meddens AJH, Karl JW, Stahl AT (2024) Evaluating a novel approach to detect the vertical structure of insect damage in trees using multispectral and three-dimensional data from drone imagery in the northern rocky mountains, USA. Remote Sens 16(8):1365. https://doi.org/10.3390/rs16081365

Silva CA, Hudak AT, Vierling LA, Loudermilk EL, O'Brien JJ, Hiers JK, Jack SB, Gonzalez-Benecke C, Lee H, Falkowski MJ, Khosravipour A (2016) Imputation of individual longleaf pine (*Pinus palustris* Mill.) tree attributes from field and LiDAR data. Can J Remote Sens 42(5):554–573. https://doi.org/10.1080/07038992.2016.1196582

Spies TA, Hemstrom MA, Youngblood A, Hummel S (2006) Conserving old-growth forest diversity in disturbance-prone landscapes. Conserv Biol 20(2):351–362. https://doi.org/10.1111/j.1523-1739.2006.00389.x

Stitt JM, Hudak AT, Silva CA, Vierling LA, Vierling KT (2022a) Characterizing individual tree-level snags using airborne lidar-derived forest canopy gaps within closed-canopy conifer forests. Meth Ecol Evol 13(2):473–484. https://doi.org/10.1111/2041-210X.13752

Stitt JM, Hudak AT, Silva CA, Vierling LA, Vierling KT (2022b) Evaluating the use of lidar to discern snag characteristics important for wildlife. Remote Sens 14(3):720. https://doi.org/10.3390/rs14030720

Strobl C, Boulesteix AL, Kneib T, Augustin T, Zeileis A (2008) Conditional variable importance for random forests. BMC Bioinformatics 9:307. https://doi.org/10.1186/1471-2105-9-307

Terho M, Hantula J, Hallaksela AM (2007) Occurrence and decay patterns of common wood-decay fungi in hazardous trees felled in the Helsinki City. For Pathol 37(6):420–432. https://doi.org/10.1111/j.1439-0329.2007.00518.x

Thomas JW, Anderson RG, Maser C, Bull EL (1979) Snags. In: Thomas JW (ed) Wildlife habitats in managed forests: the Blue Mountains of Oregon and Washington. USDA Forest Service, Agriculture Handbook No. 553, Washington, D.C., pp 60–77.

Tomback DF, Sprague E (2022) The national whitebark pine restoration plan: restoration model for the high elevation five-needle white pines. For Ecol Manag 521:120204. https://doi.org/10.1016/j.foreco.2022.120204

Varo-Martínez MÁ, Navarro-Cerrillo RM (2021) Stand delineation of *Pinus sylvestris* L. plantations suffering decline processes based on biophysical tree crown variables: a necessary tool for adaptive silviculture. Remote Sens 13(3):436. https://doi.org/10.3390/rs13030436

Vierling KT, Saab VA, Tobalske BW (2020) Lewis's woodpecker (*Melanerpes lewis*), version 1.0. In: Poole AF (ed) Birds of the world. Cornell Lab of Ornithology, Ithaca, NY, USA. https://doi.org/10.2173/bow.lewwoo.01

Volney WJA (1998) Ten-year tree mortality following a jack pine budworm outbreak in Saskatchewan. Can J for Res 28(12):1784–1793. https://doi.org/10.1139/x98-147

Wickman BE (1963) Mortality and growth reduction of white fir following defoliation by Douglas-fir tussock moth. USDA Forest Service, Pacific Southwest Forest and Range Experiment Station, Berkeley, CA

Wickman BE (1978) Tree mortality and top-kill related to defoliation by Douglas-fir tussock moth in the Blue Mountains outbreak. USDA Forest Service, Pacific Northwest Forest and Range Experiment Station, Portland, OR

Wing BM, Ritchie MW, Boston K, Cohen WB, Olsen MJ (2015) Individual snag detection using neighborhood attribute filtered airborne lidar data. Remote Sens Environ 163:165–179. https://doi.org/10.1016/j.rse.2015.03.013

Woods AJ (2014) Warmer and wetter might not be better. J for Sci 60(11):484–486. https://doi.org/10.17221/18/2014-JFS

WYaoPKrzystekMHeurich2012Identifying standing dead trees in forest areas based on 3d single tree detection from full waveform lidar dataISPRS Ann Photogramm Remote Sens Spatial Inf Sci I-710.5194/isprsannals-i-7-359-2012Yao W, Krzystek P, Heurich M (2012) Identifying standing dead trees in forest areas based on 3d single tree detection from full waveform lidar data. ISPRS Ann Photogramm Remote Sens Spatial Inf Sci I-7. https://doi.org/10.5194/isprsannals-i-7-359-2012

Youngblood A, Max T, Coe K (2004) Stand structure in eastside old-growth ponderosa pine forests of Oregon and northern California. For Ecol Manag 199(2–3):191–217. https://doi.org/10.1016/j.foreco.2004.05.056

Yu R, Luo YQ, Zhou Q, Zhang XD, Wu DW, Ren LL (2021) A machine learning algorithm to detect pine wilt disease using UAV-based hyperspectral imagery and LiDAR data at the tree level. Int J Appl Earth Obs Geoinf 101:102363. https://doi.org/10.1016/j.jag.2021.102363

Zhou Q, Yu LF, Zhang XD, Liu YJ, Zhan ZY, Ren LL, Luo YQ (2022) Fusion of UAV hyperspectral imaging and LiDAR for the early detection of EAB stress in ash and a new EAB detection index—$NDVI_{(776,\ 678)}$. Remote Sens 14(10):2428. https://doi.org/10.3390/rs14102428

Journal of Forestry Research (2026) 37:81
https://doi.org/10.1007/s11676-026-02000-7

CORRECTION

Correction: Methods for identifying topkill in conifers using airborne lidar to monitor structural diversity and disturbance

Brent W. Oblinger[1] · Benjamin C. Bright[2] · Andrew T. Hudak[2] · Kerri T. Vierling[3]

Correction to: Journal of Forestry Research (2026) 37:34
https://doi.org/10.1007/s11676-025-01979-9

The article "Methods for identifying topkill in conifers using airborne lidar to monitor structural diversity and disturbance", written by Brent W. Oblinger, Benjamin C. Bright, Andrew T. Hudak and Kerri T. Vierling, was originally published under the copyright "This is a U.S. Government work and not under copyright protection in the US; foreign copyright protection may apply". As a result of the subsequent decision to publish the article under the open access model, the article's copyright notice was changed on 16 January 2026 to © The Author(s) 2026 and the article is now distributed under a Creative Commons Attribution 4.0 International License, which permits use, sharing, adaptation, distribution and reproduction in any medium or format, as long as you give appropriate credit to the original author(s) and the source, provide a link to the Creative Commons licence, and indicate if changes were made. The images or other third party material in this article are included in the article's Creative Commons licence, unless indicated otherwise in a credit line to the material. If material is not included in the article's Creative Commons licence and your intended use is not permitted by statutory regulation or exceeds the permitted use, you will need to obtain permission directly from the copyright holder. To view a copy of this licence, visit http://creativecommons.org/licenses/by/4.0

The original article has been corrected.

The original article can be found online at https://doi.org/10.1007/s11676-025-01979-9.

✉ Brent W. Oblinger
brent.oblinger@usda.gov

[1] Forest Health Protection, USDA Forest Service, 63095 Deschutes Market Rd, Bend, OR 97701, USA

[2] Rocky Mountain Research Station, USDA Forest Service, 1221 South Main St, Moscow, ID 83844, USA

[3] Department of Fish and Wildlife Sciences, University of Idaho, 875 Perimeter Drive, Moscow, ID 83844, USA

Published online: 07 March 2026